ASEAN Engineering Journal

Full Paper

SITE-SPECIFIC DISAGGREGATION ANALYSIS OF RECENT EARTHQUAKE ON THE AMBON COAST

Kusmanto[ab], Sito Ismanti [c*], Angga Fajar Setiawan [c]

[a]Natural Disaster Management Engineering, Department of Civil and Environmental Engineering, Gadjah Mada University, Indonesia
[b]Settlement Infrastructure Agency for the East Nusa Tenggara Region, Ministry of Works and Housing, Indonesia
[c]Department of Civil and Environmental Engineering, Gadjah Mada University, Indonesia

Article history
Received
29 May 2023
Received in revised form
03 January 2024
Accepted
12 January 2024
Published online
31 August 2024

*Corresponding author
sito.ismanti@ugm.ac.id

Graphical Abstract

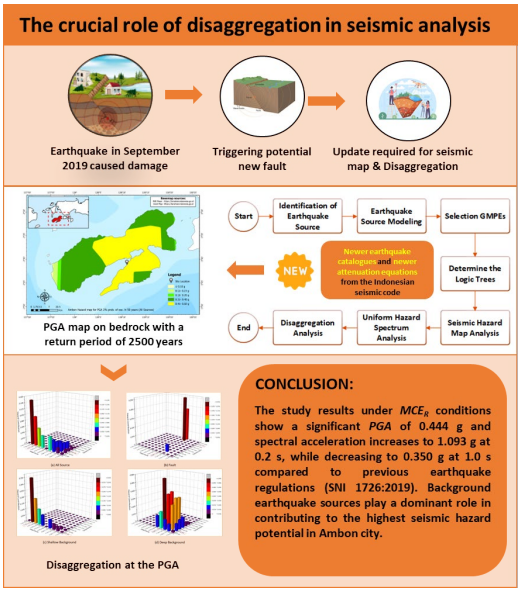

Abstract

Seismic activity in the eastern region of Indonesia, particularly in Ambon, has been a matter of great concern because of its high tectonic activity. The devastating magnitude 6.5 earthquake in September 2019, which resulted in fatalities and significant damage, highlighted the region's vulnerability and emphasized the importance of understanding the area's seismic hazards. Although previous studies have been conducted, this study aims to fill critical gaps in the literature by using the latest seismic data until 2022 and updated attenuation equations. Disaggregation analysis is employed to identify ground motion characteristics, that are crucial for calculating synthetic ground motion acceleration. Under risk-targeted maximum considered earthquake (MCE_R) conditions, the study results show a peak ground acceleration of 0.444 g, with spectral acceleration at 0.2 s reaching 1.093 g, which decreases to 0.350 g at 1.0 s. Notably, background earthquake sources play a dominant role in contributing to the region's high seismic hazard potential. The results of this study highlight the urgency of updating Indonesia's national seismic hazard map. The study also recommends future studies to explore additional parameters of newly discovered faults to enhance understanding of fault movements and their impacts in the study area.

Keywords: probabilistic, seismic risk, uniform hazard spectrum, disaggregation, background earthquakes

© 2024 Penerbit UTM Press. All rights reserved

1.0 INTRODUCTION

The eastern region of Indonesia is a highly active tectonic zone, that requires additional seismic data to understand this phenomenon. On September 26, 2019, a 6.5 magnitude earthquake occurred in the Ambon region at a depth of 10 km, causing several fatalities and damages [1]. According to the Meteorology, Climatology, and Geophysics Agency's Disaster Mitigation Earthquake and Tsunami Division, this event was influenced by the newly discovered Kawa Strike-Slip Fault Belt, also known as the "Kawa Fault," as the epicenter of the earthquake was located directly on this fault line. Many active faults cross the high terrace sea in Amahai, Ambon, and the surrounding islands, thereby creating complex tectonic events in the Ambon Coastal Area. Active faults in Ambon can cause earthquakes with magnitudes of 6.4 M_w or higher [2]. In addition, the 34 km long Ambon Fault could cause a major earthquake affecting the central city of Maluku Province, Ambon at any time. Furthermore, this fault also allows the northern part of the Banda Arc and Papua New Guinea to move east–northeast [2]. Therefore, more recent seismic studies are required to gain a better understanding of the tectonic activities in this region.

Irsyam et al. (2007) [3] conducted a seismic hazard analysis for all provinces in Indonesia using outdated attenuation equations, focusing only on disaggregation analysis for Jakarta. In a subsequent study published by Asrurifak et al. (2010) [4], more recent seismic data were utilized, revealing an increased *PGA* for a 2,500-year return period, ranging from 1.2 to 3.0 times higher than that estimated previously. Subsequently, the National Earthquake Study Center (PUSGEN) [5] conducted

research using attenuation equations and new seismic data from 2017. In 2021, PUSGEN created a disaggregation map; however, it still used pre-2017 earthquake data and excluded the September 2019 earthquake in the analysis [6]. To address this issue, the current study uses the latest seismic data up to 2022 and updated attenuation equations to provide a more accurate assessment of the seismic hazards in Ambon.

The city of Ambon requires earthquake-resistant construction planning because of its susceptibility to seismic activities. Analyzing disaggregation is crucial in this regard because it helps identify the characteristics of ground motion, which are required to calculate synthetic soil movement velocities in the area. The availability of ground motion records in Ambon, Indonesia, has become increasingly important, particularly after the M_w 6.5 earthquake in 2019, which highlighted the seismic hazards posed by the Ambon Fault [7]. The refinement of regional earthquake catalogs and seismic load designs for infrastructure projects in the surrounding area also emphasizes the importance of understanding the seismic hazards in Ambon [8].

Therefore, conducting disaggregation analyses in Ambon is crucial for accurate and effective earthquake-resistant construction planning. For this reason, the current study aims to establish a relationship between the findings of seismic risk analysis and specific earthquake records by determining the magnitude (M) and distance (R) that dominate several calculated seismic sources. The magnitude and distance data are then used as inputs for scaling the amplitude or spectral matching to identify historical records that demonstrate characteristics similar to the desired conditions.

2.0 METHODOLOGY

Seismic disaggregation is used to decompose the seismic hazard contributions from various sources into different parameters, such as magnitude, source mechanism, and epicenter distance [9]. The analysis of seismic disaggregation involves identifying seismic sources, creating seismic activity models, determining attenuation functions, and using logic trees to address parameter uncertainties [10]. In the current study, a seismic hazard map and a uniform hazard spectrum were created to represent seismic hazard distributions. The mechanism of seismic disaggregation analysis used in this study is shown in Figure 1.

2.1 Identification of Earthquake Sources

2.1.1 Earthquake Catalog

According to Ambraseys (2002) [11], certain areas that are currently experiencing seismic activity may also have experienced seismic activity 2,500 years ago. Therefore, a comprehensive and standardized earthquake inventory must be used to conduct seismic hazard analyses at each location. Teguh (2011) [12] used the United States Geological Survey (USGS) [13] earthquake database, which had a magnitude range of 5, depth of 250 km, and distance to the epicenter of 500 km. Makrup et al. (2010) [10] utilized the earthquake catalog of the Bulletin of the International Seismological Center (ISC) [14] to generate earthquake maps for Indonesia in 2010, with magnitude ranges of 5.20–9.20 for all earthquake source zones. Sunardi (2015) [15] used the USGS earthquake catalog to produce synthetic ground acceleration in Yogyakarta with a radius of 500 km for five earthquakes with a maximum depth of 300 km.

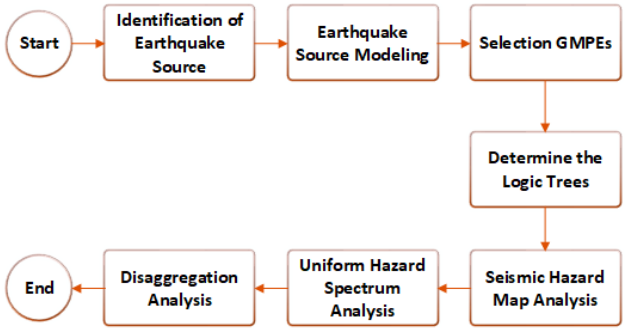

Figure 1 Study flowchart

This study generated a new inventory of instrumentally recorded earthquakes by integrating the USGS and ISC catalogs (Figure 2). The foundational concept of seismic risk lies in that fact that earthquakes occur as independent events; hence, the catalog should not include dependent events, such as foreshocks and aftershocks, to forecast future seismic activity [16]. Before clustering earthquakes, earthquake magnitudes must first be standardized, because there are multiple magnitude scales for earthquake data. In this study, the magnitude scale was standardized using the equation in Table 1 to convert it into a moment magnitude scale (M_w).

One of the most effective ways to identify the main earthquake sources is to remove foreshocks and aftershocks, a process commonly known as declustering. In this study, the delustering process was performed using the ZMAP v.7 software. We removed the foreshocks and aftershocks from the catalog using the method employed by Gardner and Knopoff (1974) [17], as shown in Figures 3 and 4. Based on the 2017 earthquake map of Indonesia [5], the method of Gardner and Knopoff (1974) works well for carrying out declustering processes.

Table 1. Correlation of magnitude scale conversion [5]

Conversion	Magnitude	Consistency (R^2)
M_w= 1.0107 M_b + 0.0801	3.7 ≤ Ms≤ 8.2	0.6975
M_w= 0.6016 M_s + 2.476	2.8 ≤ Ms≤ 6.1	0.8013
M_w= 0.9239 M_s + 0.5671	6.2 ≤ Ms≤ 8.7	0.8013

Moreover, insufficient earthquake data can lead to an inaccurate assessment of earthquake risk because the parameters may be either too high or too low. Therefore, analysis must be conducted to ensure the comprehensiveness of earthquake recording data [4]. Furthermore, to establish the duration for which a seismic catalog is deemed sufficiently comprehensive, the rate of occurrence of individual earthquakes across different magnitude ranges over time must be charted, extending from the most recent observation time to the past. This process is often referred to as the magnitude of completeness (M_c).

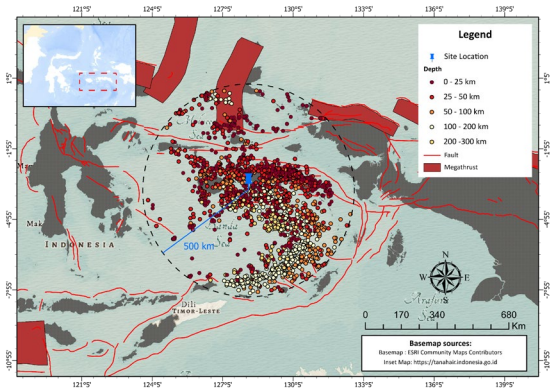

Figure 2 Modified earthquake catalog from the *USGS* [13] and *ISC Bulletin* [14]

M_c is a crucial parameter in determining the *a-value* and *b-value*, as it reflects the level of completeness of the data, which in turn, influences the extent to which the data can be considered complete [18]. In this study, we obtained the M_c, *a-value*, and *b-value* from the seismic catalog using ZMAP v.7 and the Gardner and Knopoff (1974) method. ZMAP v.7 is a valuable tool for studying seismic data, because it can be used to perform both traditional and advanced seismological analyses, making the process more accessible and informative for researchers [19].

2.1.2 Seismic Model And Seismic Parameter

Identifying and characterizing seismic source zones are of paramount importance in the evaluation of earthquake hazards. In this study, seismic zones were determined by examining tectonic, geological, and seismological factors. Considering all earthquake sources is important when conducting seismic analysis. Thus, this study employs an approach incorporating a model that includes various seismic sources, such as shallow crustal, background, and subduction.

2.1.2.1 Shallow Crustal

In the domain of seismic source modeling, the present investigation focuses on using fault geometry for identification. The 2017 earthquake map of Indonesia [5] shows a line of probabilistic analysis variables, including fault tracing, slip rate, focal mechanism, dip, length, width, and depth (Table 2). However, several fault parameters remain unidentified, thus requiring the use of empirical correlations to establish the relationship between the magnitude (*M*), fault area (*A*), fault width (*W*), and fault length (*L*) [20], as presented in Equations 1–3. According to Hanks and Kanamori (1979) [21], the long-term slip rate is regulated by the recurrence intervals of significant earthquakes along the fault. These are shown in Equations 4–6:

$$Log\,(A) = M - 4; \sigma_A = 0 \quad (1)$$

$$Log\,(W) = 0.5 * M - 2.15; \sigma_W = 0 \quad (2)$$

$$Log\,(L) = 0.5 * M - 1.85; \sigma_L = 0 \quad (3)$$

$$M_w = \frac{2}{3} log\, M_0 - 16.05 \quad (4)$$

$$\lambda\,(M) = \frac{M_o}{\mu\, L\, W\, s} \quad (5)$$

$$Log\,(M_0) = 1.5M + 16.05 \quad (6)$$

where λ(M) represents the annual number of earthquakes with magnitude M, M_0 represents the seismic moment, μ is equal to 3.0×10^{11} dyne/cm^2 and represents the shear modulus, *L* is the length of the fault, *W* is the width of the fault in kilometers, and *s* is the slip rate in centimeters per year. In addition, from the *b-value* obtained using the ZMAP v.7 program, we derived the parameters β, M_c, and M_{max} by identifying seismic sources up to 30 *km* from the fault epicenter. Table 3 lists the input parameters of the linear earthquake source zone.

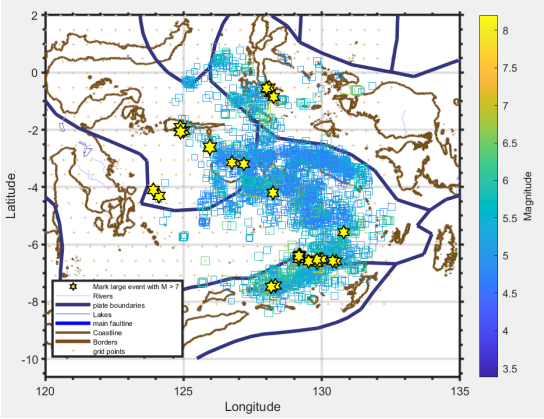

Figure 3 Earthquake catalog before declustering

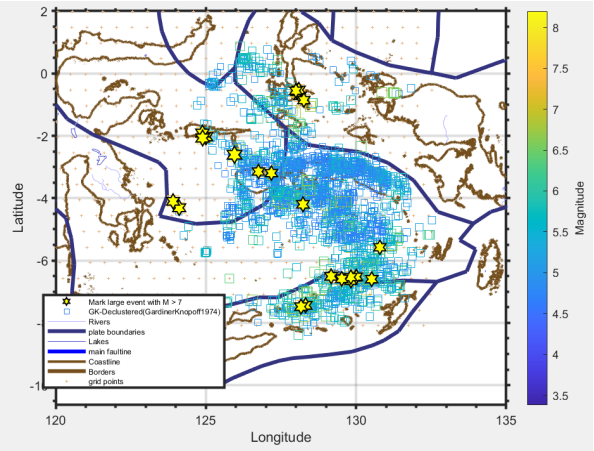

Figure 4 Earthquake catalog after declustering according to the Gardner and Knopoff (1974) method [17]

2.1.2.2 Background

A series of earthquakes have occurred in the vicinity of the city of Ambon, but the cause of the seismic activities remains undetermined (unidentified fault rupture). The components of the background earthquake sources are shown in Table 4. The background earthquake source model encompasses two distinct regions: a shallow background zone (depth ≤ 50 km) and a deep background zone (depth > 50 km) according to Makrup et al. (2010) [10]. We were able to distinguish these zones using the *a-value, b-value*, M_c, and M_{max} parameters of ZMAP v.7.

Table 2 Seismic parameters of the fault zone [5]

Zone	Mechanism	M_{max}	Slip rate (mm/year)	Dip (°)	Top (km)	*W* (km)	*L* (km)
North Buru	SS	7.40	0.50	90	3.00	18.00	100.00
Buru 2	SS	7.00	0.50	90	3.00	18.00	91.00
South Buru	SS	7.40	0.50	90	3.00	18.00	152.00
Manipa	SS	7.40	0.50	90	3.00	18.00	100.00
Taluti Strike-Slip	SS	7.10	0.50	90	3.00	18.00	54.00
Taluti Thrust	SS	6.80	0.50	45S	3.00	18.00	28.00
Gorong 1	SS	7.00	0.50	90	3.00	18.00	92.00
Gorong 2	SS	6.90	0.50	90	3.00	18.00	73.00
Bobot	SS	7.50	0.50	90	3.00	18.00	115.00
Seram Ftb1-west	TF	8.20	15.00	45SW	3.00	18.00	514.00
Seram ft2-east	TF-SS	7.40	10.00	60SW	3.00	18.00	81.00
North Wahai	SS	7.40	5.00	90	3.00	18.00	100.00
North Kobi	SS	6.80	1.00	90	3.00	18.00	30.00
North Hote	SS	7.30	5.00	90	3.00	18.00	84.00
East Bula	SS	7.10	5.00	90	3.00	18.00	51.00
West Gorom	SS	6.80	5.00	90	3.00	18.00	31.00
East Gorom	SS	7.60	5.00	90	3.00	18.00	149.00

Table 3 Seismic input R-CRISIS for the linear zone

Zone	M_c	*b-value*	σ_b	M_0 (dyne/cm²)	A (km²)	β	σ_β	λ *(M)*
North Buru	7.30	0.91	0.12	1.00E+27	1.80E+13	2.10	0.27	0.000270
Buru 2	6.90	0.76	0.09	2.51E+26	1.64E+13	1.75	0.21	0.000978
South Buru	7.30	0.76	0.09	1.00E+27	2.74E+13	1.75	0.21	0.000410
Manipa	7.30	0.80	0.11	1.00E+27	1.80E+13	1.85	0.25	0.000270
Taluti Strike Slip	7.00	1.34	0.16	3.55E+26	9.72E+12	3.09	0.36	0.000411
Taluti Thrust	6.70	1.20	0.14	1.26E+26	5.04E+12	2.75	0.32	0.000601
Gorong 1	6.90	1.23	0.14	2.51E+26	1.66E+13	2.84	0.31	0.000989
Gorong 2	6.80	1.23	0.14	1.78E+26	1.31E+13	2.84	0.31	0.001108
Bobot	7.40	1.17	0.13	1.41E+27	2.07E+13	2.70	0.30	0.000220
Seram Ftb1-west	7.90	1.15	0.13	7.94E+27	9.25E+13	2.64	0.29	0.005241
Seram ft2-east	7.30	1.18	0.13	1.00E+27	1.46E+13	2.71	0.31	0.004374
North Wahai	7.30	1.18	0.13	1.00E+27	1.80E+13	2.71	0.31	0.002700
North Kobi	6.70	1.18	0.13	1.26E+26	5.40E+12	2.71	0.31	0.001287
North Hote	7.20	1.18	0.13	7.08E+26	1.51E+13	2.71	0.31	0.003204
East Bula	7.00	1.18	0.13	3.55E+26	9.18E+12	2.71	0.31	0.003881
West Gorom	6.70	1.18	0.13	1.26E+26	5.58E+12	2.71	0.31	0.006649
East Gorom	*7.50*	*1.18*	*0.13*	*2.00E+27*	*2.68E+13*	*2.71*	*0.31*	*0.002016*

Note: λ (M) is the annual occurrence rate; parameters M_c, *b-value*, and σ_b are from ZMAP v.7; parameter β is *b log (10)*; σ_β is σ_b x log (10); *A* is the rupture area (*L* × *W*); and M_0 is the shear modulus (3.0 x 10^{11} dyne/cm²).

Table 4 Seismic input R-CRISIS for the areal zone

Zona	M_{max}	σ_{Mmax}	M_c	*a*	*b*	σ_b	β	σ_β	*N* (M_o)	*T (Year)*	λ_o	$\lambda_{(M)}$
Shallow background (0-50 *km*)	7.25	0.95	5.52	6.51	0.86	0.11	1.97	0.26	1,204.01	122	9.87	0.48
	7.30	0.74	5.09	7.72	1.15	0.14	2.65	0.32	1,293.92	122	10.61	0.58
	7.47	0.73	5.41	5.78	0.73	0.09	1.68	0.20	708.43	122	5.81	0.53
Deep background (50-100 *km*)	7.27	0.93	5.48	6.54	0.86	0.12	1.99	0.27	1,209.97	122	9.92	0.50
Deep background (100-300 *km*)	7.19	0.21	5.57	6.70	0.89	0.11	2.04	0.25	1,417.83	122	11.62	0.46
Subduction	7.40	0.00	5.59	5.88	0.72	0.10	1.65	0.23	1,011.40	122	8.29	0.57
	7.07	0.33	5.42	5.93	0.79	0.08	1.81	0.18	612.77	122	5.02	0.36

Note: *λ (M)* is the annual occurrence rate; parameters M_{max}, σ_{Mmax}, M_c, *b-value*, and σ_b are from ZMAP v.7; *β* is *b* × log (10); and σ_β is σ_b × log (10).

Subsequently, we segregated the data based on prior grouping using ArcGIS Pro. The maximum likelihood method elucidates the relationship between the frequency and magnitude of earthquakes. According to Pasau and Tanauma (2011) [22], the maximum likelihood statistical analysis of earthquake parameters provides more reliable results because it incorporates the slope of the average Gaussian distribution function rather than a minor square fitting of the magnitude:

$$Log\ N\ (M_o) = a - b.M_o \quad (7)$$

$$\lambda_0 = \frac{N(M_o)}{T} \quad (8)$$

where $N(M_0)$ is the number of earthquakes with a magnitude of *M* or greater, and *M* is the moment magnitude with M_o = 4 as the lowest moment magnitude (M_w). In addition, the *a*- and *b-values* are constants, *T* is the recording time in the earthquake catalog, and λ_o is the annual frequency of earthquakes with magnitudes equal to M_o. The earthquake magnitude was

calculated on the basis of the modified Gutenberg–Richter model described by Cornell and Vanmarcke (1969)[23]:

$$\lambda(M) = \lambda_0 \frac{\exp(-\beta M) - \exp(-\beta M_{max})}{\exp(-\beta M_o) - \exp(-\beta M_{max})}, M_o \leq M \leq M_u \quad (9)$$

where β is $b \times \log(10)$, M_{max} is the highest magnitude, and $\lambda(M)$ is the annual number of earthquakes equal to M.

2.1.2.3 Subduction

A seismic activity zone known as a "subduction zone" emerges in a region where oceanic plates converge with continental plates. In this study, we delineate and analyze this zone using the *a-value*, *b-value*, M_c, and M_{max} parameters derived from the ZMAP v.7 software. Two specific subduction zones, Megathrust Philippine and Megathrust Papua, served as earthquake sources for this investigation. The optimal depth for earthquake sources is generally considered to be 50 km [4]. Table 4 presents a list of the input parameters necessary for subduction earthquake sources. In this study, we used R-CRISIS, a software that can import source geometry and seismicity parameters using ESRI shape files to facilitate the importation of earthquake sources [24].

2.2 Selection Ground Motion Prediction Equations

Ground-motion prediction equations (*GMPEs*) are critical tools for estimating the intensity of ground motions during earthquakes. These equations consider various factors, such as earthquake magnitude, soil properties, and distance from the earthquake source to the site. In this study, we used empirically developed *GMPEs* using specific regression methods to calculate the probability distribution of the ground motion intensity. Table 5 lists the *GMPEs* used in this study. The *GMPEs* for the faults and shallow backgrounds are the same as those used in the Indonesian earthquake map. In contrast, we used Parker (2020)-NGA 2 [25] for subduction and deep backgrounds as it incorporates more data sources than NGA subduction. This equation is applicable to subduction earthquakes at interfaces and intralabs in various regions, including Japan, Taiwan, Cascadia, Mexico and the rest of Central America, South America, the Aleutian Islands, and Alaska [25].

Table 5 Ground motion prediction equations (*GMPEs*)

Source	GMPEs	Weight
Fault and Shallow background	Boore et al. (2014)	0.33
	Campbell and Bozorgnia (2014)	0.33
	Chiou and Youngs (2014)	0.34
Subduction (Interface)	Parker (2020)-NGA 2 model interface	0.33
	Youngs (1997)-Interface	0.33
	Zhao (2006)-Interface	0.34
Benioff (deep background)	Parker (2020)-NGA 2 model interslabs	0.33
	Youngs (1997)-Interslabs	0.33
	Zhao (2006)-Interslabs	0.34

2.3 Logic Trees

Logic trees are commonly used to represent and quantify epistemic uncertainty in each element of seismic sources and ground motion prediction models [26]. Several approaches or models can be employed in the analysis using logic trees, each with a weight factor that demonstrates how to prioritize it over others. Here, the sum of the weight factors of each parameter must equal one. Owing to the limitations of the observational data, we weighed four types of seismogenic source models and three sets of *GMPEs*, as shown in Figure 5.

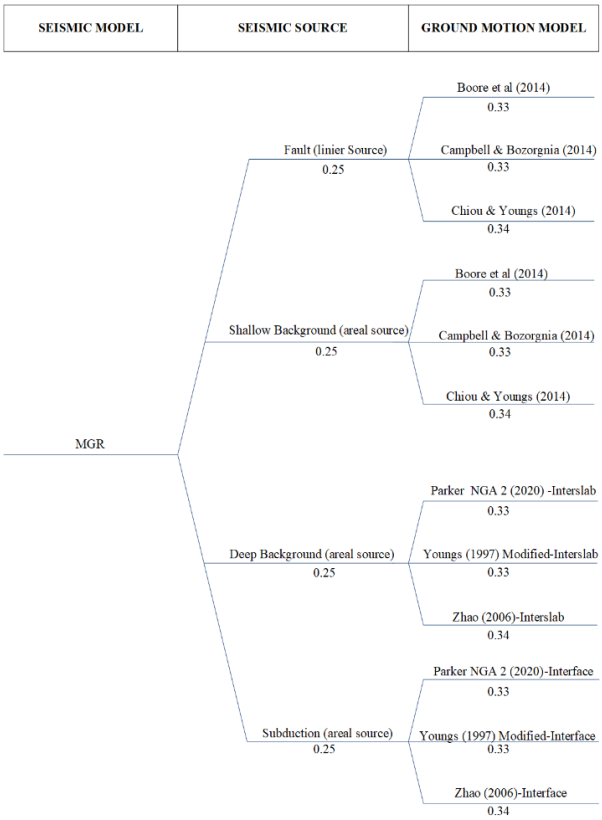

Figure 5 Modified logic trees for all source models [21]

2.4 Seismic Hazard Map and Uniform Hazard Spectrum

This study used a grid system with a resolution of 0.1° × 0.1° to assess earthquake hazards. Then, to determine the peak ground acceleration (*PGA*) and spectrum acceleration, calculations were conducted at the center of each grid by employing the parameters of the entire area of interest. By analyzing these values, scientists can estimate the likelihood of an earthquake occurring in a specific region. The use of smaller grid sizes allows for a more refined evaluation of earthquake danger. Furthermore, this study sought to identify the contribution of each potential source within a 300 km radius of the center of each grid cell to the overall risk value.

The R-CRISIS program is a powerful tool used in the current study to generate a uniform hazard spectrum. This was accomplished by inputting the parameters of the various seismic sources. The software boasts exceptional computational efficiency and the ability to select from a range of models [27]. Meanwhile, we also used the Cornell (1968) [28] method to

analyze seismic hazards in the region and for the lines of seismic sources. We also assumed that earthquakes would occur uniformly within each unit area of the initial region and that all points were considered as potential sources of seismic activity. Furthermore, we used R-CRISIS to perform spatial integration by dividing the seismic sources and calculating accurate hazard estimates.

2.5 Seismic Hazard Disaggregation

Disaggregation of seismic hazards is a crucial means for identifying factors causing seismic hazards at a specific location [29]. Such an analysis provides deep insights into the types of earthquakes with the highest potential hazards based on the location and time of occurrence [30]. By detailing seismic hazard characteristics (e.g., ground movement) or earthquake parameters (e.g., magnitude and distance), this technique allows for the identification of earthquakes that contribute the most to the probability or occurrence of certain ground motion intensities [31].

Seismic hazard disaggregation involves calculating the percentage contributions of various seismic sources to the hazard for a particular time interval [32]. This method is commonly used to select ground motions for structural analyses [33]. Reliable source calculations, such as the *USGS* National Seismic Hazard Model, enhance accuracy in this field [34]. Furthermore, seismic hazard disaggregation plays a vital role in mapping earthquake design, understanding the characteristics of a specific region, identifying significant events, and determining the appropriate specifications for ground motion selection and scaling procedures [35].

In this study, we conducted disaggregation analysis using the R-CRISIS software with magnitudes ranging from 4 to 8 and distances ranging from 0 to 400 km. First, we collected data on seismic hazards, including earthquake records, seismic occurrence parameters, and specific location information [36]. Subsequently, we identified the parameters for disaggregation, including the magnitude, proximity to the location, and intensity of the ground motion [29]. Next, we used the R-CRISIS software for disaggregation—a process that involved executing specific scripts or functions within the software [37]. Once the disaggregation is completed, the results can be used to analyze and understand the contributions of different seismic sources to the overall hazard at the study location [30]. At this point, the results must be validated to ensure consistency with existing methodologies and expected patterns [38].

3.0 RESULTS AND DISCUSSION

3.1 Seismic Hazard Map

In this study, we produced newer seismic hazard maps for peak ground accelerations at periods of 0.2 s and 1.0 s, with a critical damping factor of 5% and a 2% probability of exceedance for 50 years. The spectral acceleration values obtained from Figures 6 to 8 are summarized in Table 6. The spectral acceleration generated by All Source were 0.42 g at *PGA*, 0.97 g at 0.2 s, and 0.28 g at 1 s. These values are all lower than those in the Indonesian National Standard map (SNI 03-1726-2019) [39], which shows 1.084 g at 0.2 s and 0.39 g at 1.0 s. Such a difference is due to the fact that the earthquake map in SNI 03-1726-2019 [39] was already under risk-targeted maximum considered earthquake (MCE_R) conditions, whereas the spectral acceleration generated in this study did not consider this. Therefore, to reach the MCE_R condition, the Uniform Hazard Spectrum (*UHS)* must be multiplied by the directivity factor (D_f) and risk coefficient (C_r).

In addition, as shown in Table 6, the spectral acceleration values for the peak ground acceleration (*PGA*) or period 0 *s* were similar for the shallow and deep backgrounds, with a value of 0.31 *g*. However, for the short (0.2 *s*) and long (1.0 *s*) periods, the spectral acceleration values in the deep background were larger than those in the shallow background, with values of 0.74 *g* and 0.62 *g*, respectively. These results indicate that Ambon City is affected by the two most dominant earthquake types, namely, deep background and shallow background.

Table 6 Results of spectral acceleration (*SA*)

Source	Spectral Acceleration (*g*)		
	PGA	**0.2 s**	**1.0 s**
All Source	0.42	0.97	0.28
Fault	0.13	0.26	0.12
Shallow Background	0.31	0.62	0.17
Deep Background	0.31	0.74	0.21
Subduction	0.01	0.01	0.01

3.2 Uniform Hazard Spectrum

This study used the R-CRISIS program to create a *UHS* based on input parameters from earthquake sources at a return period of 2500 years. This study assumes that earthquakes occur uniformly in each unit area within the initial region and that all points are considered potential earthquake sources. We also used R-CRISIS in this study to perform spatial integration by dividing earthquake sources to produce an accurate hazard estimation. As shown in Figure 9, the background earthquake source was the largest contributor in this study, with a *PGA* value of 0.31 *g*, a period of 0.2 *s* of 0.74 *g*, and a period of 1.0 *s* of 0.21 *g*. Meanwhile, the subduction earthquake source showed the smallest spectral acceleration value (0.01 *g* for all periods). This can be attributed to the location of the earthquake source being very far from the study site; therefore, the study area is not affected.

The results also showed that the background earthquake source was the most dominant source at the study location. This is because this area experiences earthquakes that are large in magnitude and with relatively high frequencies, but the source of the earthquakes remain unknown. Similarly, Tasikmalaya, Indonesia, has the most dominant background earthquake source [40], indicating that studies identifying earthquake sources in the Indonesian region have not been widely conducted. Therefore, it is necessary to conduct studies in other Indonesian cities to update the national seismic hazard maps. Meanwhile, to compare the *UHS* with the MCE_R determined by SNI 03-1726-2019 [30], the *UHS* generated in this study must consider the directivity factor (D_f) at a probability level exceeding 2% over 50 years with 5% attenuation. The value of D_f is equal to 1.0 when period (T) = 0 s, 1.1 when T = 0.2 s, and 1.3 when T = 1 s. D_f can be calculated linearly between T = 0 s and T = 0.2 s and between T = 0.2 s and T = 1.0 s. When T > 1.0 s, D_f = then 1.3 applies [41].

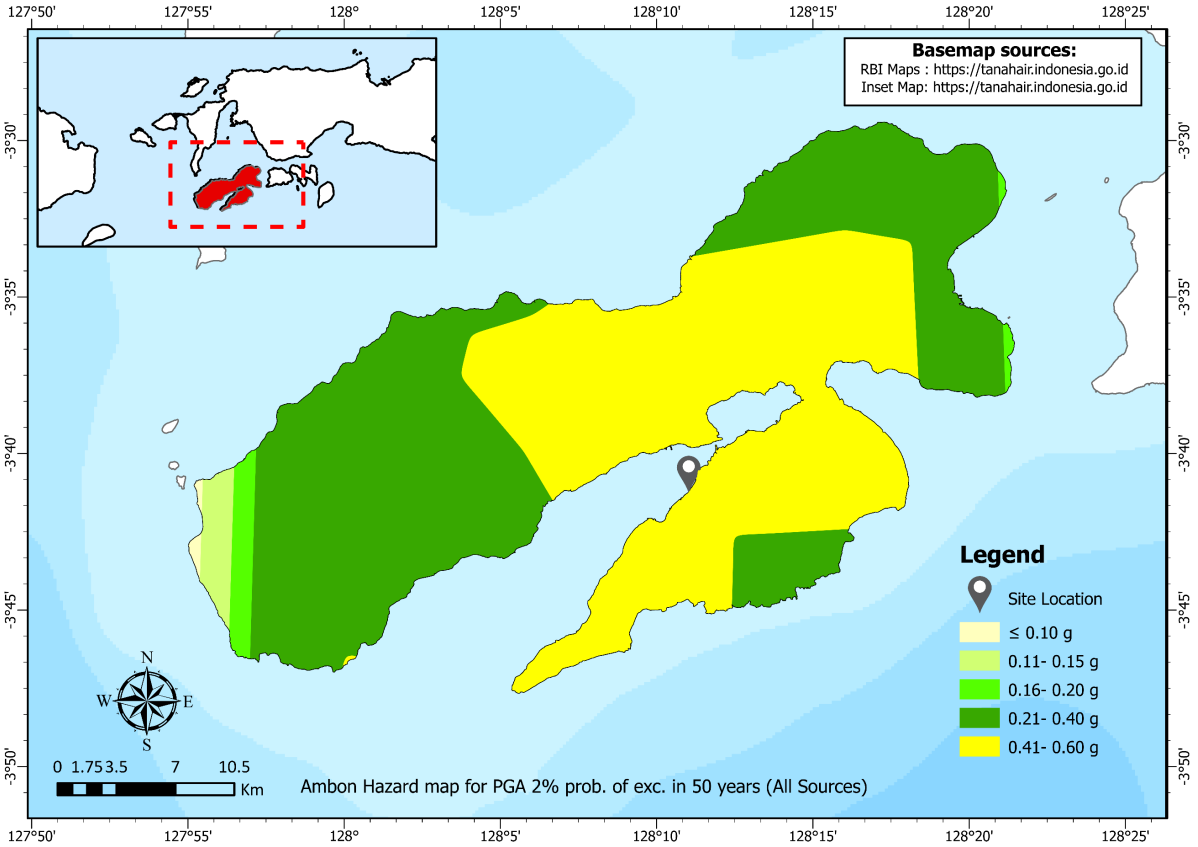

Figure 6 Peak ground acceleration map on bedrock with a return period of 2500 years (all sources)

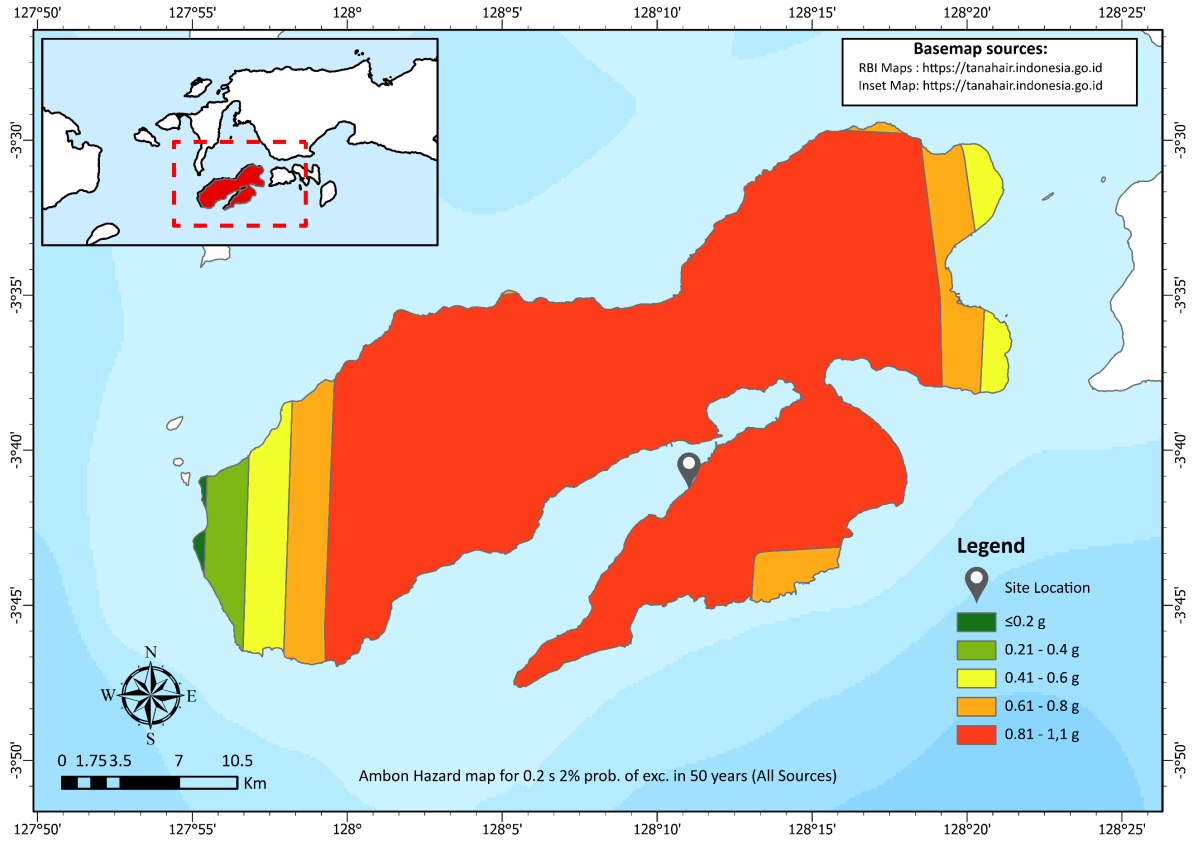

Figure 7 0.2 s spectral acceleration map with a return period of 2500 years (all sources)

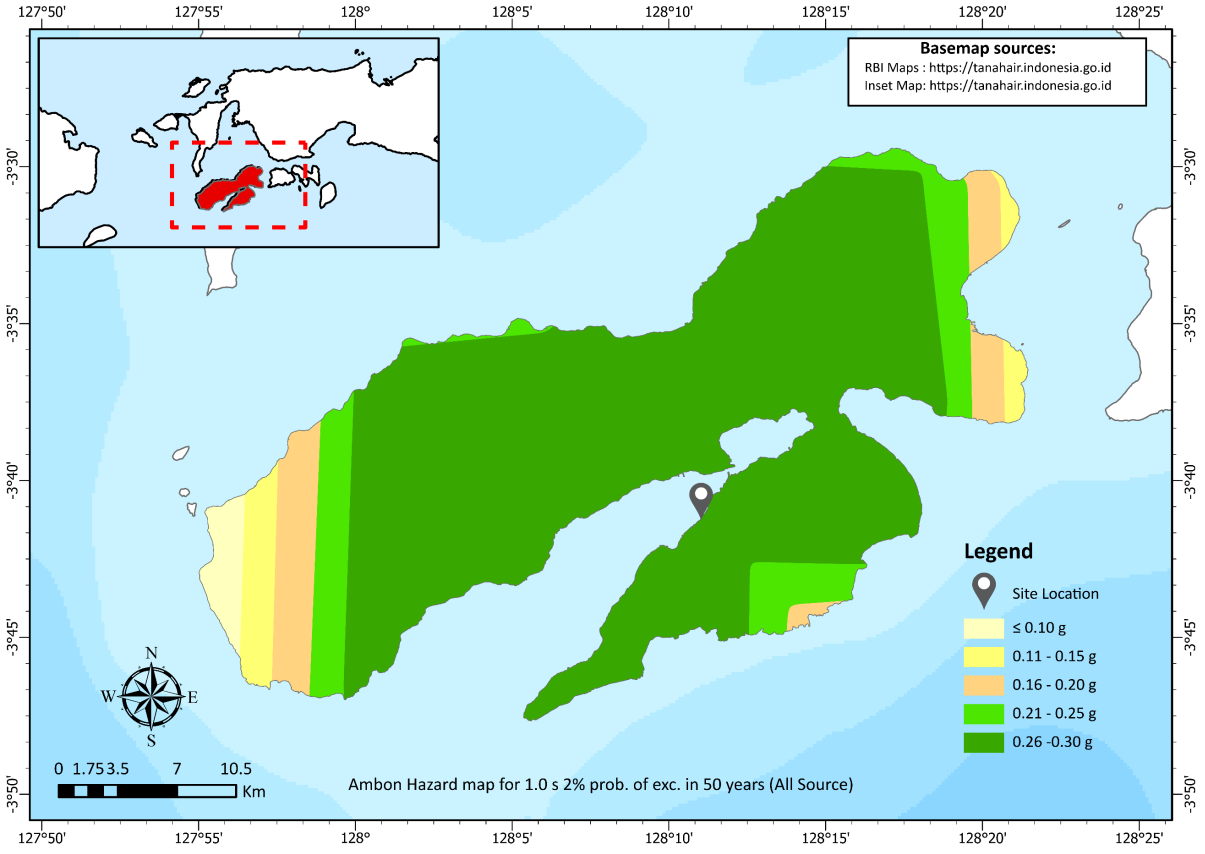

Figure 8 1.0 s spectral acceleration map with a return period of 2500 years (all sources)

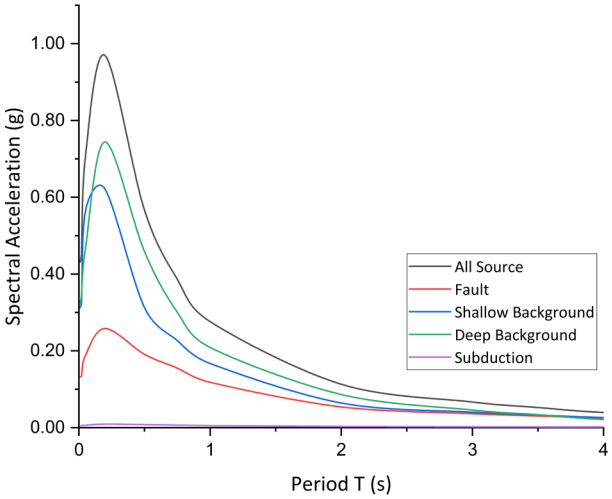

Figure 9 Uniform hazard spectrum

Aside from the importance of the directivity factor, it should be noted that building collapse with a 50-year maximum considered earthquake (*MCE*) level cannot be assumed to be uniform. Thus, we also considered the target risk coefficient (C_R) to distribute the risk evenly and obtain the spectral acceleration corresponding to the MCE_R condition [39]. We then calculated the risk coefficient (C_R) using C_{RS} and C_{R1} values. For periods less than or equal to 0.2 s, C_R should be equal to C_{RS}, whereas for periods greater than 1 s, C_R should be equal to C_{R1}. The C_R value is determined using the linear interpolation of the C_{RS} and C_{R1} values for spectral acceleration periods greater than 0.2 s but less than 1.0 s. The results of *the UHS*-to-MCE_R conversion in this study are presented in Table 7. As can be seen, the calculated peak ground acceleration is 0.444 g, the spectral acceleration at a period of 0.2 s is 1.093 g, and the spectral acceleration at 1.0 s is 0.350 g. Furthermore, the results reveal that the spectral acceleration values increased at periods close to 0.2 s but decreased thereafter (Figure 10). Finally, the results show that the site-specific hazard curve for short-period spectral acceleration in Ambon City is greater than that of SNI 03-1726-2019 [39].

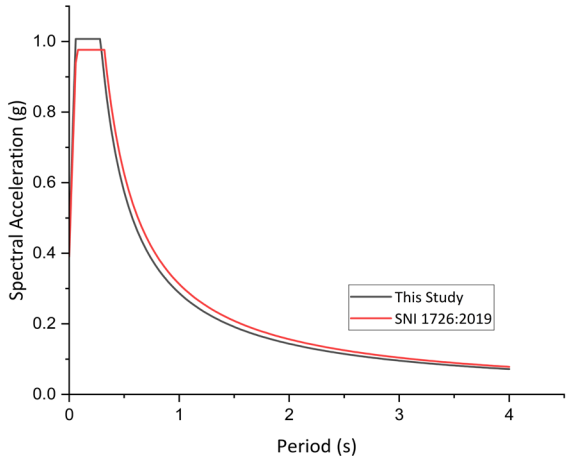

Figure 10 Comparison between the study results and modified MCE_R-based SNI 03-1726-2019 [39]

Table 7 Calculated MCE_R from the *UHS*

Period, T (s)	*SA* (g)	C_R	D_f	MCE_R
0.00	0.43	1.025	1.005	0.444
0.02	0.45	1.025	1.010	0.469
0.05	0.71	1.025	1.025	0.742
0.20	0.97	1.025	1.100	1.093
0.50	0.57	1.006	1.175	0.670
0.75	0.39	0.991	1.238	0.474
1.00	0.28	0.975	1.300	0.350
2.00	0.11	0.975	1.300	0.143
3.00	0.07	0.975	1.300	0.084
3.50	0.05	0.975	1.300	0.066
4.00	0.04	0.975	1.300	0.050
5.00	0.03	0.975	1.300	0.035

3.3 Disaggregation Analysis

In this study, we used the R-CRISIS software to determine the contribution of the disaggregation process to earthquake hazards in the city of Ambon, as shown in Figures 11–13. In addition, Table 8 shows that during the 0.2 s period, the dominant magnitude (M_D) of shallow background earthquake sources ranged from 5.67 to 5.96, with a dominant distance (R_D) of 0–30 km. For deep background earthquake sources, the M_D was also in the same range of 5.67 to 5.96, but with an R_D of 60–90 km. In the 1.0 s period, the M_D of shallow background earthquake sources ranged from 6.25 to 6.55, with an R_D of 0–30 km. For deep background earthquake sources, the M_D also ranged from 7.42 to 7.71, but with *an* R_D of 90–120 km. The results obtained in this study differ from the disaggregation map produced by PUSGEN [6], particularly for the 0.2 s period, where the dominant magnitude for shallow faults is between 6 and 6.2 with a dominant distance of 40–50 km. Meanwhile, for beniof or intraplate earthquakes, the dominant magnitude ranged between 7.2 and 7.4, with a dominant distance of 100–120 km.

The disaggregation results showed that the earthquake that occurred in September 2019 with magnitudes of 6.5 and 28.1 km from the study site was the dominant earthquake over a long period. Therefore, the earthquake had a significant impact on tall buildings [42]. The significant impact of the September 2019 Ambon earthquake on buildings caused severe damage to residential buildings and public facilities. The National Disaster Management Agency reported that more than 6,000 buildings were damaged, with 41 fatalities and 1,578 injuries [43]. Therefore, this analysis is relevant to recent conditions, because the findings can be used as a reference in building design, especially for high-rise buildings in Ambon city.

In this study, the megathrust in the Philippines and Papua was identified as a source of subduction earthquakes. However, the R-CRISIS software cannot display the M_D and R_D for subduction earthquakes because the resulting spectral acceleration is negligible. Due to their distance from the source, the impact of subduction earthquakes at the study site is considered negligible, even though they generally have potential magnitudes above M_w > 8. [24]. Furthermore, although large earthquakes can also spread far and wide, their wave energy tends to weaken with increasing distance from the source. Therefore, its impact on areas far from the subduction zone is negligible compared with its impact on areas close to the subduction zone.

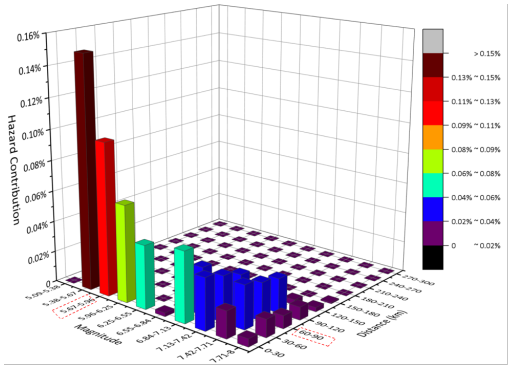

(a) All Source

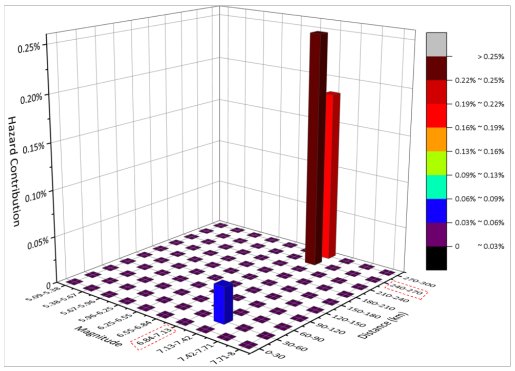

(b) Fault

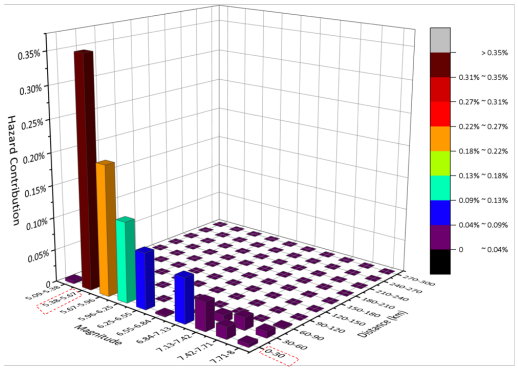

(c) Shallow Background

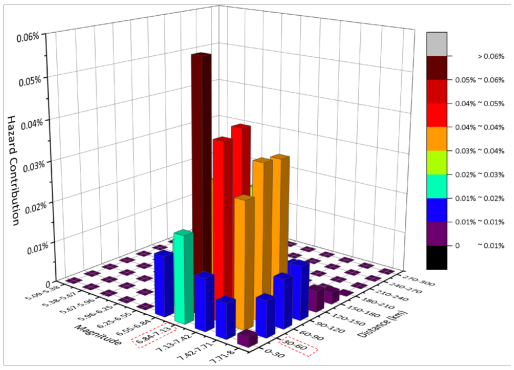

(d) Deep Background

Figure 11 Disaggregation at the *PGA*

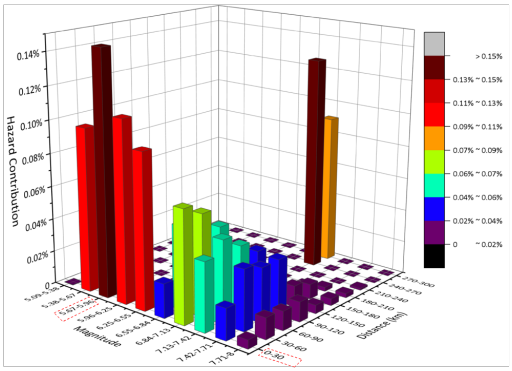

(a) All Source

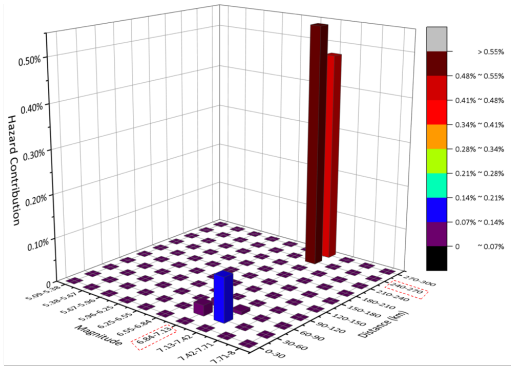

(b) Fault

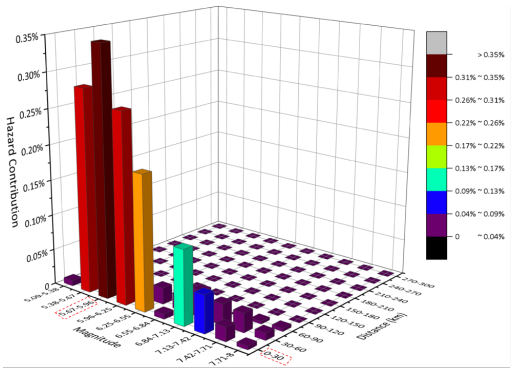

(c) Shallow Background

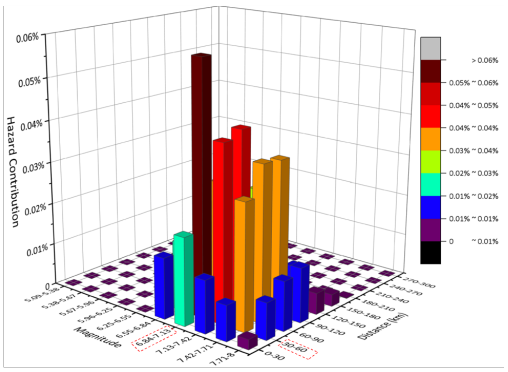

(d) Deep Background

Figure 12 Disaggregation at 0.2 s

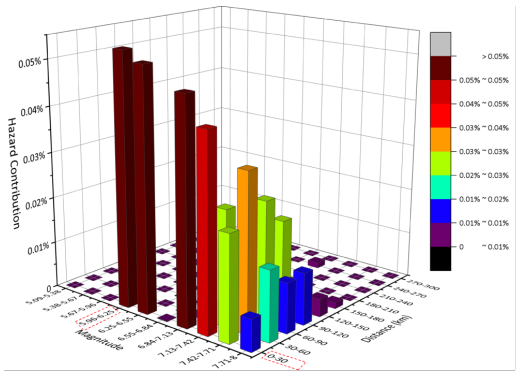

(a) All Source

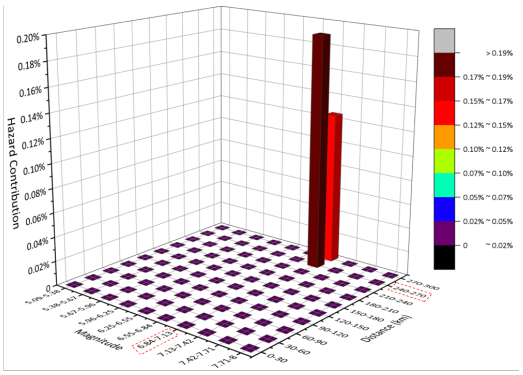

(b) Fault

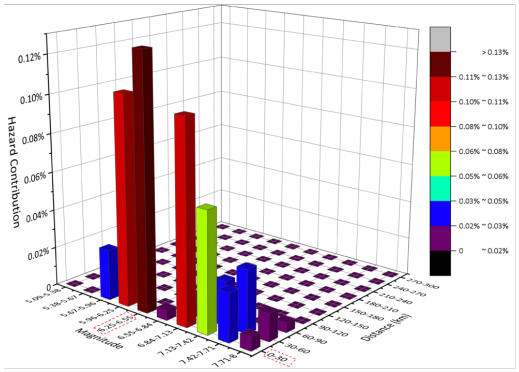

(c) Shallow Background

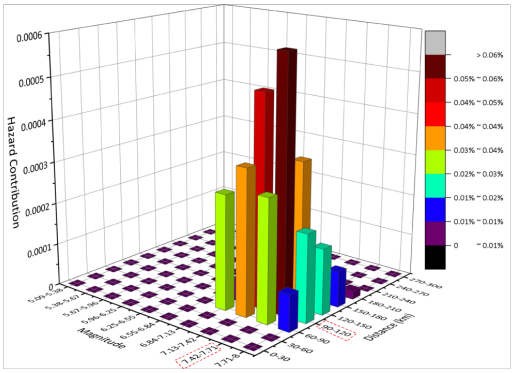

(d) Deep Background

Figure 13 Disaggregation at 1.0 s

Table 8 Dominant magnitude (M_D) and dominant distance (R_D)

Sources	*PGA*		SA 0.2 *s*		SA 1.0 *s*	
	M	R (km)	M	R (*km*)	M	R (*km*)
All Source	5.38–5.67	0–30	5.67–5.96	0–30	5.96–6.25	0–30
Fault	6.84–7.13	240–270	6.84–7.13	240–270	6.84–7.13	240–270
Shallow Background	5.38–5.67	0–30	5.67–5.96	0–30	6.25–6.55	0–30
Deep Background	6.84–7.13	30–60	7.42–7.71	60–90	7.42–7.71	90–120

The results also showed that the contribution of faults to the potential earthquake hazard in Ambon City was relatively small for all periods. This is because the previously studied faults are located approximately 60 km from the study area. Thus, we were unable to consider the finding of a new potential fault by Patria (2021) [2] in Amahai, Ambon City, which could have produced an earthquake of magnitude M_w 6.9. Information on the parameters of these potential faults remains limited. Further studies are needed to obtain more complete parameters, including width, area, and annual slip rate, thus gaining a better understanding of the fault's potential seismic hazard. Moreover, to obtain information on fault movement, direct global positioning system (*GPS*) measurements and morphological analyses must also be conducted to understand the shape and pattern of the land surface surrounding the fault.

4.0 CONCLUSION

In this study, the *UHS* shows higher values for shorter durations and lower values for longer durations under MCE_R conditions compared with the spectral response outlined in SNI 03-1726-2019. Background earthquakes significantly affect the seismic activity in Ambon City, in which shallow background earthquakes causing higher spectral acceleration for short periods, whereas deep background earthquakes produce larger spectral acceleration for long periods. This study identified two earthquake catalogues, one from the *USGS* and one from the *ISC*, covering the period of 1900–2022. We also determined earthquake source parameters, including those from faulting and subduction, on the basis of SNI 03-1726-2019 and the findings of more recent studies. Furthermore, the R-CRISIS tool was used to generate seismic hazard maps, uniform hazard spectra, and site-specific disaggregation of the Ambon data.

The spectral acceleration values generated by the all source were 0.42 g at *PGA*, 0.97 g at 0.2 *s*, and 0.28 g at 1 s. These values are lower than those specified in the SNI 03-1726-2019 map, i.e., 1.084 g at 0.2 s and 0.39 g at 1.0 s. However, under the MCE_R condition, the peak ground acceleration was 0.444 *g*, and the spectral acceleration rates at 0.2 and 1.0 s were 1.093 and 0.35 g, respectively. These results indicate increased spectral acceleration at 1 s, as well as increased spectral acceleration for short periods and a decrease for long periods.

The results of this study demonstrate that background earthquake sources have the most dominant contribution in generating earthquake hazards at the study site. The fact that this region has experienced large magnitude and high-frequency earthquakes while the source remains unknown highlights the need for further studies to update Indonesia's national seismic hazard map. In addition, the impact of the September 2019 earthquake in Ambon can provide empirical validation of the analysis, indicating that the hazard curves obtained in this analysis are consistent with recent events.

The results underscore the urgent need to build structures capable of withstanding high spectral acceleration during long periods caused by background earthquakes. The findings also provide a basis for the selection of ground motion for performance-based analysis in Ambon. Furthermore, the results emphasize the importance of updating seismic hazard maps and national building design codes to reflect updated data on current seismic activities. To expand the findings of this study, future research should identify additional parameters of the potential new faults discovered by Patria (2021), such as area, extent, and annual slip rate, to aid better hazard evaluation. Finally, further *GPS* measurements and morphological analyses are required to obtain more accurate information on the fault movement and its impact on the study area.

Acknowledgements

We express our sincere appreciation to the Ministry of Public Works and Housing as well as the Settlement Infrastructure Agency for the Maluku Region for their indispensable support in providing the data and assisting us in various aspects of this article. Our gratitude also extends to Universitas Gadjah Mada for their invaluable assistance through the Language Editing Service. University support significantly enhanced the scope and efficacy of our research.

References

[1] Marasabessy, M., Pallu, M. S., Lopa, R. T., & Thaha, M. A. 2020. Development of flood forecasting model and warning systems at Way Ruhu – Ambon. *IOP Conference Series: Earth and Environmental Science*. 419(1): 012115. DOI: http://dx.doi.org/10.1088/1755-1315/419/1/012115

[2] Patria, A., Tsutsumi, H., & Natawidjaja, D. H. 2021. Active fault mapping in the onshore northern Banda Arc, Indonesia: Implications for active tectonics and seismic potential. *Journal of Asian Earth Sciences*. 218: 1–13. DOI: http://dx.doi.org/10.1016/j.jseaes.2021.104881

[3] Irsyam, M., Dangkua, D. T., Kusumastuti, D., & Kertapati, E. K. 2007. Methodology of Site-Specific Seismic Hazard Analysis for Important Civil Structure. *Petra Civil Engineering Journal*. 9(2). Available: https://ojs.petra.ac.id/ojsnew/index.php/civ/article/view/16657/16649

[4] Asrurifak, M., Irsyam, M., Budiono, B., Hendriyawan, H., & Triyoso, W. 2010. Development of Spectral Hazard Map for Indonesia with a Return Period of 2500 Years using Probabilistic Method. *Civil Engineering Dimension*. 12(1): 52–62. DOI: http://dx.doi.org/10.9744/ced.12.1.52-62

[5] National Earthquake Study Center (PUSGEN) and Housing and Settlement Research and Development Center, Eds. 2017. *Indonesia Earthquake Source and Hazard Map 2017, First Edition*. Bandung: Center for Housing and Settlement Research and Development, Research and Development Agency, Ministry of Public Works.Available: https://simantu.pu.go.id/content/?id=3605. Accessed: May 01, 2023.

[6] National Earthquake Study Center (PUSGEN). 2022. *Earthquake Disaggregation Book 2022 For Planning and Evaluation of Earthquake*

Resistant Infrastructure. Ministry of Public Works and Housing. Available: http://perpus.ditbtpp.id/digital/buku/detail/2208. Accessed: May 23, 2023.

[7] Meilano, I. et al. 2021. Source characteristics of the 2019 Mw 6.5 Ambon, Eastern Indonesia, earthquake inferred from seismic and geodetic data. *Seismological Research Letters*. 92(6): 3339–3348. DOI: http://dx.doi.org/10.1785/0220210021

[8] Kamaruddin, B., Sahara, D. P., & Halauwet, Y. 2022. Refining the regional aftershocks catalog of the Ambon earthquake Mw 6.5 on 26 September 2019 using manual picking and a non-linear algorithm: Preliminary result. *Journal of Physics: Conference Series*. 2243(1): 012014. DOI: http://dx.doi.org/10.1088/1742-6596/2243/1/012014

[9] Bazzurro, P., & Cornell, C. A. 1999. Disaggregation of seismic hazard. *Bulletin of the Seismological Society of America*. 89(2): 501–520. DOI: http://dx.doi.org/10.1785/BSSA0890020501

[10] Makrup, L. L., Irsyam, M., Sengara, I. W., & Hendriyawan, H. 2010. Hazard Deaggregation for Indonesia. *Jurnal Teknik Sipil Insitut Teknologi Bandung*. 17(3): 181. DOI: http://dx.doi.org/10.5614/jts.2010.17.3.4

[11] Ambraseys, N. 2002. The Seismic Activity of the Marmara Sea Region over the Last 2000 Years. *Bulletin of the Seismological Society of America*. 92(1): 1–18. DOI: http://dx.doi.org/10.1785/0120000843

[12] Teguh, M. 2011. Proposed Synthetic Ground Motion of Yogyakarta Region. *Universitas Islam Indonesia*. 11(1): 9–15. Available: https://publikasiilmiah.ums.ac.id//handle/11617/1929

[13] USGS. Accessed May 24, 2023. Available: https://earthquake.usgs.gov/earthquakes/search

[14] ISC Bulletin. Accessed May 24, 2023. DOI: https://doi.org/10.31905/D808B830

[15] Sunardi, B. 2015. Synthetic Ground Acceleration of Yogyakarta City Based on Earthquake Hazard Deaggregation. *Journal of Geology and Mining*. 6(3). Available: http://jlbg.geologi.esdm.go.id/index.php/jlbg/article/view/85/85

[16] Peterson, C., & Seligman, M. E. P. 2004. *Character strengths and virtues: A handbook and classification*. Washington, DC: American Psychological Association; Oxford University Press. Available: https://psycnet.apa.org/record/2004-13277-000

[17] Gardner, J. K., & Knopoff, L. 1974. Is the sequence of earthquakes in Southern California, with aftershocks removed, Poissonian?. *Bulletin of the Seismological Society of America*. 64 (5): 1363–1367. DOI: https://doi.org/10.1785/BSSA0640051363

[18] Elhuda, I., Agustawijaya, D. S., & Sulistiyono, H. 2018. Evaluation of Earthquake Territory in Lombok using Statistical Method. *International Journal of Emerging Trends in Science and Technology*. 5(1). DOI: http://dx.doi.org/10.18535/ijetst/v5i1.05

[19] [19] Wiemer, S. 2001. A Software Package to Analyze Seismicity: ZMAP. *Seismological Research Letters*. 72(3): 373–382. DOI: http://dx.doi.org/10.1785/gssrl.72.3.373

[20] Singh, S. K., Bazan, E., & Esteva, L. 1980. Expected earthquake magnitude from a fault. *Bulletin of the Seismological Society of America*. 70(3): 903–914. DOI: http://dx.doi.org/10.1785/BSSA0700030903

[21] Hanks, T. C., & Kanamori, H. 1979. A moment magnitude scale. *Journal of Geophysical Research*. 84(B5): 2348. DOI: http://dx.doi.org/10.1029/JB084iB05p02348

[22] Pasau, G., & Tanauma, A. 2011. Modelling Earthquake Sources in the North Sulawesi Region as an Earthquake Disaster Mitigation Effort. *Jurnal Ilmu Sosial.* 15(1): 202. DOI: http://dx.doi.org/10.35799/jis.11.2.2011.208

[23] Cornell, C. A., & Vanmarcke, E. H. 1969. The Major Influences on Seismic Risk. *Proceedings of the 4th World Conference on Earthquake Engineering, Santiago, Chile*. A1:69–83. Available: http://www.iitk.ac.in/nicee/wcee/article/4_vol1_A1-69.pdf

[24] Ordaz, M., Salgado-Gálvez, M. A., & Giraldo, S. 2021. R-CRISIS: 35 years of continuous developments and improvements for probabilistic seismic hazard analysis. *Bulletin of Earthquake Engineering.* 19(7): 2797–2816. DOI: http://dx.doi.org/10.1007/s10518-021-01098-w

[25] Parker, G. A., Stewart, J. P., Boore, D. M., Atkinson, G. M., & Hassani, B. 2022. NGA-subduction global ground motion models with regional adjustment factors. *Earthquake Spectra*. 38(1): 456–493. DOI: http://dx.doi.org/10.1177/87552930211034889

[26] Bommer, J. J. 2012. Challenges of Building Logic Trees for Probabilistic Seismic Hazard Analysis. *Earthquake Spectra*. 28: 1723–1735. DOI: http://dx.doi.org/10.1193/1.4000079

[27] Tselentis, G.-A., & Danciu, L. 2010. Probabilistic seismic hazard assessment in Greece – Part 1: Engineering ground motion parameters. *Natural Hazards and Earth System Sciences*. 10(1): 25–39. DOI: http://dx.doi.org/10.5194/nhess-10-25-2010

[28] Cornell, C. A. 1968. Engineering seismic risk analysis. *Bulletin of the Seismological Society of America*. 58(5): 1583–1606. DOI: http://dx.doi.org/10.1785/BSSA0580051583

[29] Fonseca, J., & Vilanova, S. 2011. Comment on Sousa, M. L. and Costa, A. C., 'Ground motion scenarios consistent with probabilistic seismic hazard disaggregation analysis. Application to mainland Portugal'. *Bulletin of Earthquake Engineering.* 9(4): 1289–1295. DOI: http://dx.doi.org/10.1007/s10518-011-9275-1

[30] Barani, S., Spallarossa, D., & Bazzurro, P. 2009. Disaggregation of probabilistic ground-motion hazard in Italy. *Bulletin of the Seismological Society of America*. 99(5): 2638–2661. DOI: http://dx.doi.org/10.1785/0120080348.

[31] Iervolino, I. 2011. *Design Earthquakes and Conditional Hazard. Dolšek, M. (eds) Protection of Built Environment Against Earthquakes*. Springer, Dordrecht. DOI: http://dx.doi.org/10.1007/978-94-007-1448-9_3.

[32] Bradley, B., Cubrinovski, M., & Wentz, F. 2022. Probabilistic seismic hazard analysis of peak ground acceleration for major regional New Zealand locations. *Bulletin of the New Zealand Society for Earthquake Engineering*. 55(1): 15–24. DOI: http://dx.doi.org/10.5459/bnzsee.55.1.15-24

[33] Fox, M., Stafford, P., & Sullivan, T. 2015. Seismic hazard disaggregation in performance-based earthquake engineering: Occurrence or exceedance? *Earthquake Engineering & Structural Dynamics*.45(5): 835–842. DOI: http://dx.doi.org/10.1002/eqe.2675

[34] Baker, J., Rezaeian, S., Goulet, C., Luco, N., & Teng, G. 2021. A subset of Cybershake ground-motion time series for response-history analysis. *Earthquake Spectra*. 37(2): 1162–1176. DOI: http://dx.doi.org/10.1177/8755293020981970

[35] Peláez, J., Casado, C., & Henares, J. 2002. Deaggregation in magnitude, distance, and azimuth in the south and west of the Iberian Peninsula. *Bulletin of the Seismological Society of America.* 92(6): 2177–2185. DOI: http://dx.doi.org/10.1785/0120010295

[36] McGuire, R. 1995. Probabilistic seismic hazard analysis and design earthquakes: Closing the loop. *Bulletin of the Seismological Society of America.* 85(5): 1275–1284. DOI: http://dx.doi.org/10.1785/bssa0850051275

[37] Petersen, M. et al. 2019. The 2018 update of the US National Seismic Hazard Model: Overview of model and implications. *Earthquake Spectra.* 36(1): 5–41. DOI: http://dx.doi.org/10.1177/8755293019878199

[38] Azarbakht, A., & Douglas, J. 2022. Variations in uniform hazard spectra and disaggregated scenarios during earthquake sequences. *Bulletin of Earthquake Engineering.* 21(1): 77–94. DOI: http://dx.doi.org/10.1007/s10518-022-01540-7

[39] National Standardization Agency of Indonesia. 2019. *Indonesian Standard Code, Earthquake Resistance Design for Buildings (SNI 03-1726-2019).* Jakarta, Indonesia. Available: https://pesta.bsn.go.id/produk/detail/12762-sni17262019. Accessed: May 12, 2023.

[40] Sunardi, B. 2019. Re-Evaluation of Seismic Hazard in Tasikmalaya City Using Probabilistic Approach. *International Journal of GEOMATE*. 17(63): 187–194. DOI: http://dx.doi.org/10.21660/2019.63.60620

[41] Pawirodikromo, W., Makrup, L., Teguh, M., & Suryo, B. 2020. Development of synthetic ground motion at a specific site in Yogyakarta town, Indonesia utilizing the PSHA Method. *E3S Web Conferences*. 156 (2020) 02011: 1–10. DOI: http://dx.doi.org/10.1051/e3sconf/202015602011

[42] Gu, C. et al. 2018. Ground motion in Kuwait from regional and local earthquakes: Potential effects on tall buildings. *Pure and Applied Geophysics.* 175(12): 4183–4195. DOI: http://dx.doi.org/10.1007/s00024-018-1943-5

[43] Rakuasa, H., Karsidi, A., Rifai, A., Tambunan, M., & K, A. 2022. Spatial dynamics model of earthquake prone area in Ambon City. *IOP Conference Series: Earth and Environmental Science*, 1039(1): 012057. DOI: http://dx.doi.org/10.1088/1755-1315/1039/1/0120